1

Introduction

1.1 Natural Abundance of Elements in the Earth's Crust

1.1.1 Chemical Elements

Recent advances in $Cu(Ga,In)Se_2$ and CdTe thin-film solar cells have resulted in commercially viable photovoltaic modules. Currently, the best performing thin-film solar cells on the cell as well as on the module level are fabricated using $Cu(Ga,In)Se_2$ absorbers. Despite having superior efficiencies, $Cu(Ga,In)Se_2$ and CdTe are seemed to be not amenable for eventual terawatt- or petawatt-scale production due to the cost and/or scarcity of Cd, Ga, and In raw metals. Notice that both Ga and In are rather costly metals, about 100 times more expensive than Cu and Zn. Therefore, one major challenge for thin-film photovoltaic technology is to develop materials composed of earth-abundant and nontoxic elements.

CZTS is an emerging solar cell absorber, which is structurally similar to chalcopyrite semiconductors, such as $CuGaSe_2$, $CuInSe_2$, and $Cu(Ga,In)Se_2$, but contains only earth-abundant, nontoxic elements and has a near optimal direct band-gap energy of $E_g \sim 1.5$ eV with high optical absorption coefficients. The fact of CZTS being isoelectronic to chalcopyrite means that a number of its material properties (e.g., the crystal structure and tensor properties) are very similar to chalcopyrite semiconductors. This promises that the same preparation methods can be used and photovoltaic devices have been successfully prepared using the same device design, structure, and processing as chalcopyrite solar cells.

Table 1.1 lists the percent natural abundance for the stable nuclides in the earth's crust. Figure 1.1 also plots the abundance in the earth's crust versus atomic number for the elements from $_1$H to $_{94}$Pu. Given the first and second most abundant elements of oxygen

Earth-Abundant Materials for Solar Cells: Cu_2–II–IV–VI_4 Semiconductors, First Edition. Sadao Adachi.

Table 1.1 *Abundance of elements in the earth's crust*[a]

Z	Symbol	Crust abundant (%)	Z	Symbol	Crust abundant (%)
1	H	0.14	51	Sb	0.00002
2	He	8×10^{-7}	52	Te	1×10^{-7}
3	Li	0.002	53	I	0.000045
4	Be	0.00028	54	Xe	3×10^{-9}
5	B	0.001	55	Cs	0.0003
6	C	0.02	56	Ba	0.0425
7	N	0.0019	57	La	0.0039
8	O	46.1	58	Ce	0.00665
9	F	0.0585	59	Pr	0.00092
10	Ne	5×10^{-7}	60	Nd	0.00415
11	Na	2.36	61	Pm	
12	Mg	2.33	62	Sm	0.000705
13	Al	8.23	63	Eu	0.0002
14	Si	28.2	64	Gd	0.00062
15	P	0.105	65	Tb	0.00012
16	S	0.035	66	Dy	0.00052
17	Cl	0.0145	67	Ho	0.00013
18	Ar	0.00035	68	Er	0.00035
19	K	2.09	69	Tm	0.000052
20	Ca	4.15	70	Yb	0.00032
21	Sc	0.0022	71	Lu	0.00008
22	Ti	0.565	72	Hf	0.0003
23	V	0.012	73	Ta	0.00020
24	Cr	0.0102	74	W	0.000125
25	Mn	0.095	75	Re	7×10^{-8}
26	Fe	5.63	76	Os	1.5×10^{-7}
27	Co	0.0025	77	Ir	1×10^{-7}
28	Ni	0.0084	78	Pt	5×10^{-7}
29	Cu	0.006	79	Au	4×10^{-7}
30	Zn	0.007	80	Hg	8.5×10^{-6}
31	Ga	0.0019	81	Tl	0.000085
32	Ge	0.00015	82	Pb	0.0014
33	As	0.00018	83	Bi	8.5×10^{-7}
34	Se	0.000005	84	Po	2×10^{-14}
35	Br	0.00024	85	At	
36	Kr	1×10^{-8}	86	Rn	4×10^{-17}
37	Rb	0.009	87	Fr	
38	Sr	0.037	88	Ra	9×10^{-11}
39	Y	0.0033	89	Ac	5.5×10^{-14}
40	Zr	0.0165	90	Th	0.00096
41	Nb	0.002	91	Pa	1.4×10^{-10}
42	Mo	0.00012	92	U	0.00027
43	Tc		93	Np	
44	Ru	1×10^{-7}	94	Pu	
45	Rh	1×10^{-7}	95	Am	
46	Pd	1.5×10^{-6}	96	Cm	
47	Ag	7.5×10^{-6}			
48	Cd	0.000015			
49	In	0.000025			
50	Sn	0.00023			

Numbers show percentage in mass.

[a] W. M. Haynes (ed.), "Abundance of elements in the Earth's crust and in the sea," in *CRC Handbook of Chemistry and Physics on DVD Version 2013* (CRC Press, Boca Raton, 2013), pp. 14–18.

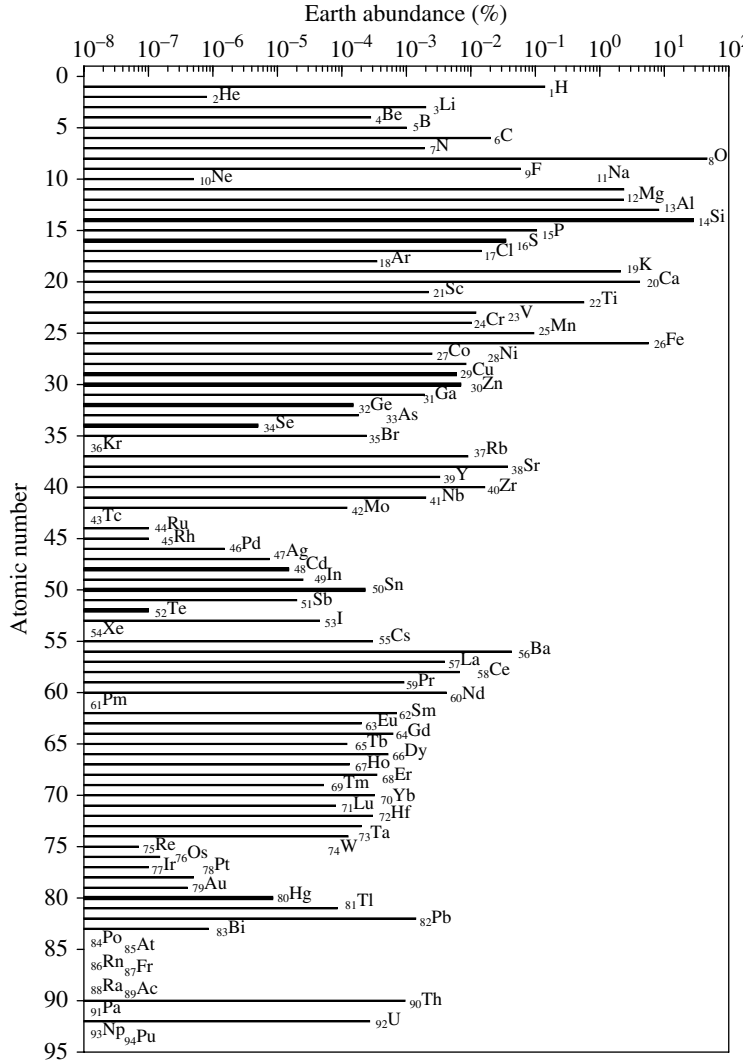

Figure 1.1 *Abundance of elements in the earth's crust*

and Si in the earth's crust (see Figure 1.1), it should not be surprising that the most abundant minerals in the crust are the silicates. Use of abundant and nontoxic elements is a great advantage; however, the requirement of thick Si absorber layers (~100 μm), due to the low absorption coefficient of this semiconductor material, combined with the typical high-temperature processing makes *c*-Si technology expensive.

Cd, Ga, and In are the 65th, 35th, and 63rd most abundant elements in the earth's crust, respectively. Cu is the 26th most abundant element in the earth's crust and occurs as native copper or in minerals such as the copper sulfides, copper carbonates, and copper oxides.

Zn is the 24th most abundant element in the earth's crust. The most common zinc ore is a ZnS (sphalerite) mineral. Sulfur (S) is also an abundant and multivalent nonmetal. S occurs in the earth naturally as the pure element and as sulfide and sulfate minerals. Tellurium and selenium have been depleted from the crust due to formation of volatile hydrides.

1.1.2 Solar Cells and Earth-Abundant Materials

Various solar cell devices exhibit varying conversion efficiencies and have varying costs. Semiconductor materials presently used or considered for photovoltaic solar cells include single-crystalline Si, polycrystalline Si, amorphous Si, GaAs, InP, CdS, CdTe, Cu–III–VI_2 chalcopyrite compounds ($CuGaS_2$, $CuInSe_2$, $Cu(Ga,In)Se_2$, etc.), and Cu_2–II–IV–VI_4 compounds (CZTS, CZTSe, etc.). Many currently available high-efficiency solar cells are made from bulk semiconductors that are cut into wafers. Thin-film layers have also been researched and shown promising properties in terms of solar cell efficiency. Si remains the only semiconductor that is well researched in both bulk and thin-film forms and also in both crystalline and amorphous phases.

We list in Table 1.2 the percent natural abundance per raw element for some interesting semiconductors used or to be used in photovoltaic applications. These specialized abundance values are calculated from the equation

$$S_a = \frac{\sum_i A_i n_i}{\sum_i n_i} \tag{1.1}$$

where A_i and n_i are the percent abundance and number of the ith element of a semiconductor, respectively. Using values of A_i listed in Table 1.1, as an example, we obtain

$$S_a = \frac{0.006 \times 2 + 0.007 + 28.2 + 0.035 \times 4}{2 + 1 + 1 + 4} = 3.5449\% \tag{1.2}$$

for Cu_2ZnSiS_4 quaternary. Recently, GaInN-based multiple quantum-well solar cells have drawn much attention due to their favorable photovoltaic characteristics, including direct and tunable band gaps covering nearly the entire solar spectrum, high absorption coefficient, high electron mobility, and superior solar radiation resistance [1]. Thus, the S_a values of GaN and InN are also listed in Table 1.2.

The largest S_a value in Table 1.2 is 28.2% for Si. CdTe is a well-known II–VI compound semiconductor. This material has the smallest S_a value of 0.000008% owing to their very small values of Cd and Te. Note that Cd present in the cells would be toxic if released. As expected, the S-based Cu_2–II–IV–VI_4 quaternaries provide larger S_a values (>3.5%) than those without containing Si (IV) element. The $S_a \sim 0.02\%$ value of CZTS is about one order larger than that of CZTSe (~0.0024%). These values are also considerably larger than that of GaAs (~0.001%) but smaller than InP value of ~0.05%.

Table 1.2 *Earth abundance per unit atom of raw elementals used for various solar cell applications (in %)*

Photovoltaic material									
IV		III–V		II–VI		Cu–III–VI_2		Cu_2–II–IV–VI_4	
Si	28.2	GaN	0.0019	CdS	0.0175	$CuGaS_2$	0.0195	Cu_2ZnSiS_4	3.5449
Ge	0.00015	GaAs	0.0010	CdTe	0.000008	$CuGaSe_2$	0.0020	$Cu_2ZnSiSe_4$	3.5274
		InP	0.0525			$CuInS_2$	0.0190	$Cu_2ZnSiTe_4$	3.5274
		InN	0.0010			$CuInSe_2$	0.0015	Cu_2ZnGeS_4	0.0199
								$Cu_2ZnGeSe_4$	0.0024
								$Cu_2ZnGeTe_4$	0.0024
								CZTS	0.0199
								CZTSe	0.0024
								$Cu_2ZnSnTe_4$	0.0024
								Cu_2CdSiS_4	3.5440
								$Cu_2CdSiSe_4$	3.5265
								$Cu_2CdSiTe_4$	3.5265
								Cu_2CdGeS_4	0.0190
								$Cu_2CdGeSe_4$	0.0015
								$Cu_2CdGeTe_4$	0.0015
								Cu_2CdSnS_4	0.0190
								$Cu_2CdSnSe_4$	0.0015
								$Cu_2CdSnTe_4$	0.0015
								Cu_2HgSiS_4	3.5440
								$Cu_2HgSiSe_4$	3.5265
								$Cu_2HgSiTe_4$	3.5265
								Cu_2HgGeS_4	0.0190
								$Cu_2HgGeSe_4$	0.0015
								$Cu_2HgGeTe_4$	0.0015
								Cu_2HgSnS_4	0.0190
								$Cu_2HgSnSe_4$	0.0015
								$Cu_2HgSnTe_4$	0.0015

Values are calculated from Equation 1.1.

1.2 Solar Radiation Spectrum

Radiation from the sun sustains life on earth and determines climate. Figure 1.2 shows the solar radiation spectra at both the top of the earth's atmosphere and sea level. The energy flow within the sun results in a surface temperature of ~5800 K, so the spectrum of the radiation from the sun is similar to that of a 5800 K blackbody with fine structures (viz., the Fraunhofer lines) due to absorption in the cool peripheral solar gas. The irradiance of the sun falling on the earth changes over a year by about 7% due to the variation in the sun–earth distance. Solar activity variations also cause changes of up to 1%.

As the sunlight passes through the atmosphere, some is absorbed by atomic and molecular gases with specific absorption lines and bands (see O_2 and H_2O in Figure 1.2). There is the ozone (O_3) layer in the lower portion of the stratosphere from ~20 to 30 km above the earth's

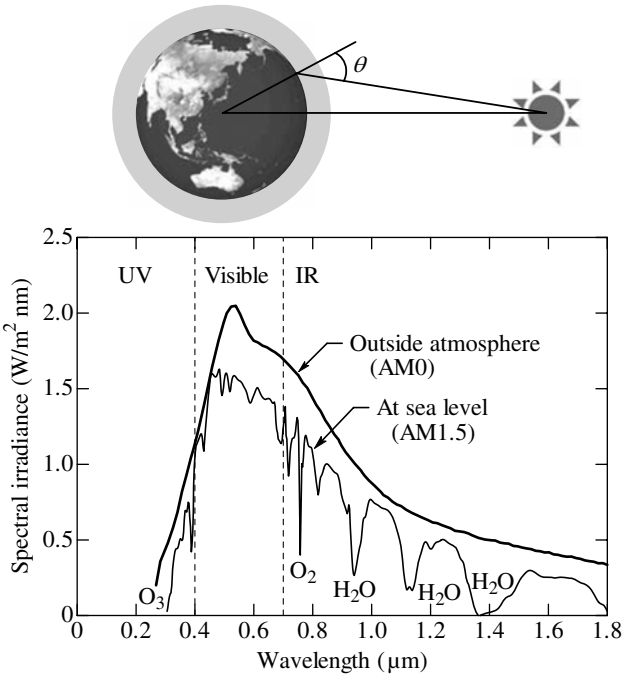

Figure 1.2 *Solar radiation spectra at both the top of the earth's atmosphere (AM0) and sea level (AM1.5)*

surface. The ozone layer absorbs ~98% of the sun's UV (200–320 nm) radiation, which otherwise would potentially damage exposed life forms on the earth. Additional light is redistributed by Rayleigh scattering $\left(I_R \propto \lambda^{-4}\right)$, which is responsible for the atmosphere's blue color.

Identification of a reference spectral irradiance for terrestrial applications is a much more difficult subject because of the abovementioned effects of the atmosphere on sunlight, which are a function of the path length through the atmosphere [2]. A way of describing an atmospheric path is called the relative optical path length, which is simplified to "air mass (AM)." To a first approximation, the AM is the secant of the solar zenith angle (see Figure 1.2). Thus, AM1 indicates the sun is directly overhead, and AM1.414 is a 45° zenith angle. The extraterrestrial solar irradiance at a distance of one astronomical unit from the sun is commonly used as a reference spectral irradiance. This irradiance corresponds to AM0 because at the top of the atmosphere, the path length is zero. The AM0 and AM1.5 spectra are shown in Figure 1.2.

1.3 Shockley–Queisser Efficiency Limit

A solar cell energy conversion efficiency is the percentage of power converted from sunlight to electrical energy under certain conditions. The efficiency limit was first calculated by Shockley and Queisser in 1961 [3] and took into consideration the solar radiation by a 6000 K blackbody. It is one of the most fundamental parameters to solar cell production.

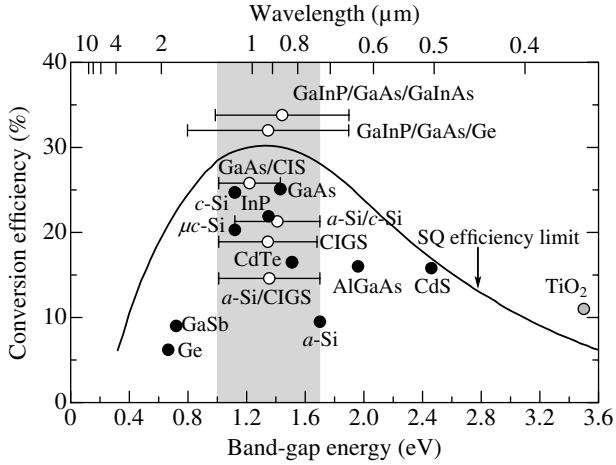

Figure 1.3 *SQ efficiency limit together with conversion efficiencies obtained from various semiconductor solar cells and dye-sensitized TiO_2 solar cell. The shaded region indicates an optimal E_g range (~1.0–1.7 eV) in the SQ efficiency limit. The solid and open circles show the results obtained from one* pn*-junction and multijunction solar cells, respectively. CIGS = $Cu(Ga,In)Se_2$*

As mentioned in Section 1.2, the solar radiation with various wavelengths reaches the earth. Not all the photons can create an electron–hole pair. The photon with energy less than the band-gap energy E_g will be transmitted without being absorbed in the semiconductor or will be converted into heat. The photon having energy higher than E_g of a semiconductor absorber can excite an electron from the VB to the CB. The photon having excessively high energy can excite electron at the highly lying CB state; however, such electron will quickly relax toward the bottom of the CB states via the electron–phonon interaction or carrier–carrier scattering.

Figure 1.3 plots the SQ efficiency limit [3]. The experimental conversion efficiency versus E_g plots, gathered from various sources, are also shown in Figure 1.3. The solar radiation has peculiar spectrum peaking at ~500 nm, as shown in Figure 1.2. Only the photon that has enough energy ($E > E_g$) to knock an electron out of its place can create an electron–hole pair. If a photon has 2.0 eV and falls onto a 1.1 eV cell, the excess energy of 0.9 eV will be lost in the form of heat. Thus, the theoretical SQ efficiency limit shows a maximum near $E_g \sim 1.3$ eV. There are a number of assumptions associated with the SQ limit that restrict its general applicability to all types of solar cells. A few of these assumptions are one semiconductor material and one *pn* junction per solar cell. The solid circles in Figure 1.3 represent the results obtained from such one *pn*-junction solar cells.

In Figure 1.3, the theoretical limit for *c*-Si solar cell is about 30%. About 50% of the solar energy gets converted to heat. About 20% of the photons pass through the solar cell. Difference of about 5% between the theoretical and experimental conversion efficiencies may account for optical losses at the surface of the cell even though it is usually textured and coated with an antireflection coating, electrical losses (e.g., Joule loss), etc.

The multijunction solar cell technology has been developed to capture more of the solar radiations than the case with conventional Si solar cells. Each multijunction solar cell is made of semiconductor layers desired to capture one range of wavelengths of sunlight. The open circles in Figure 1.3 are obtained from this type of multijunction solar cells.

1.4 Fundamental Properties of Photovoltaic Semiconductor Materials

Various semiconductors show varying conversion efficiencies and have varying costs. Semiconductor materials to be used for efficient solar cells must have characteristics matched to the spectrum of available light. Thus, the most important semiconductor properties for solar energy conversion devices are the band-gap energy E_g and optical absorption spectrum $\alpha(E)$. We summarize in Table 1.3 the crystal structure, lattice constant, and lowest band-gap energy for some group IV, III–V, II–VI, and I–III–VI_2 semiconductors. Figure 1.4 also

Table 1.3 *Crystal structure, lattice constants (a and c), and lowest band-gap energy (E_g) at 300 K for some group IV, III–V, II–VI, and I–III–VI_2 semiconductors*

System	Material	CS	Lattice constant		E_g (eV)
			a (nm)	*c* (nm)	
IV	Diamond	*d*	0.35670		5.50 (ID)
	Si	*d*	0.54310		1.12 (ID)
	Ge	*d*	0.56579		0.6657 (ID)
	3C-SiC	*zb*	0.43596		2.39 (ID)
III–V	α-GaN	*h* (*w*)	0.31896	0.51855	3.420 (D)
	GaP	*zb*	0.54508		2.261 (ID)
	GaAs	*zb*	0.565330		1.43 (D)
	GaSb	*zb*	0.609593		0.72 (D)
	InP	*zb*	0.58690		1.35 (D)
	InAs	*zb*	0.60583		0.359 (D)
	InSb	*zb*	0.647937		0.17 (D)
II–VI	ZnO	*h* (*w*)	0.32495	0.52069	3.45 (D)
	β-ZnS	*zb*	0.54102		3.726 (D)
	ZnSe	*zb*	0.56692		2.721 (D)
	ZnTe	*zb*	0.61037		2.27 (D)
	c-CdS	*zb*	0.5825		2.46 (D)
	c-CdSe	*zb*	0.6077		1.675 (D)
	CdTe	*zb*	0.6481		1.51 (D)
I–III–VI_2	$CuAlS_2$	*ch*	0.532	1.043	3.34 (D)
	$CuAlSe_2$	*ch*	0.561	1.092	2.68 (D)
	$CuAlTe_2$	*ch*	0.596	1.177	2.43 (D)
	$CuGaS_2$	*ch*	0.535	1.046	2.43 (D)
	$CuGaSe_2$	*ch*	0.561	1.100	1.68 (D)
	$CuGaTe_2$	*ch*	0.600	1.193	1.23 (D)
	$CuInS_2$	*ch*	0.552	1.108	1.53 (D)
	$CuInSe_2$	*ch*	0.578	1.155	1.01 (D)
	$CuInTe_2$	*ch*	0.617	1.234	0.99 (D)

ch, chalcopyrite; CS, crystal structure; D, direct band gap; *d*, diamond; *h*, hexagonal; ID, indirect band gap; *w*, wurtzite; *zb*, zincblende.

shows the relationships between the direct/indirect band-gap energy E_g and lattice constant a for a number of group IV, III–V, and II–VI semiconductors crystallizing in the cubic structure. The alloy bowing parameters for E_g are taken from Adachi [4]. Note that semiconductor alloys can provide us a natural means of tuning the various material parameters so as to optimize and widen the applications of semiconductor devices. The solar irradiance spectrum at AM1.5 is also shown on the right-hand side of Figure 1.4. The same relationships, but for I–III–VI_2 chalcopyrite semiconductors, are shown in Figure 1.5. Here, no

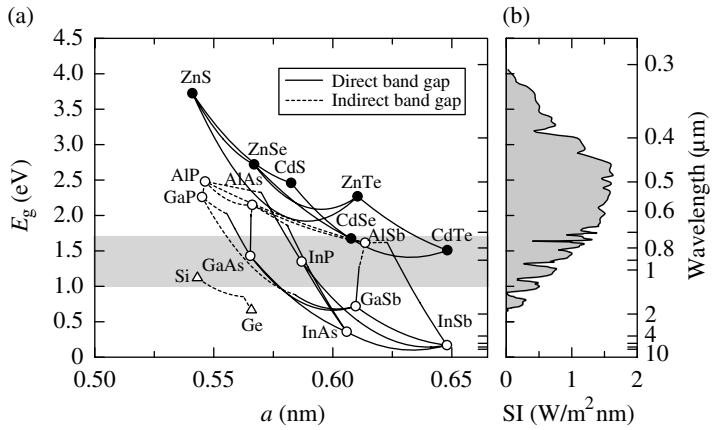

Figure 1.4 *(a) Band-gap energy* E_g *versus lattice constant* a *for a number of group IV, III–V, and II–VI semiconductors crystallizing in the cubic structure at 300 K [4]. The shaded region indicates an optimal* E_g *range (~1.0–1.7 eV) in the SQ efficiency limit (see Figure 1.3). (b) Spectral irradiance (SI) for sunlight at AM1.5*

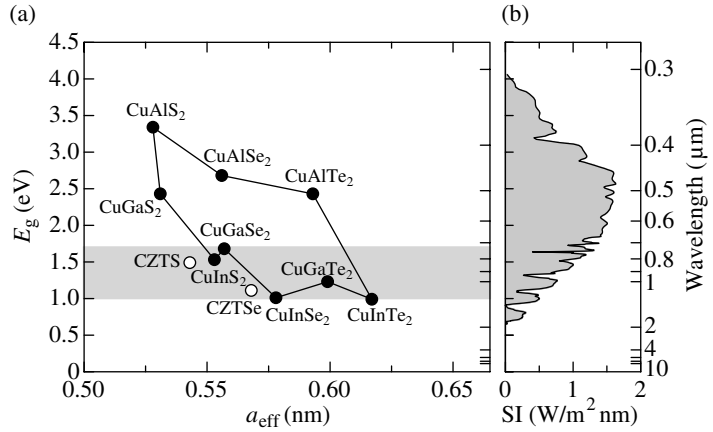

Figure 1.5 *(a) Band-gap energy* E_g *versus effective lattice constant* a_{eff} *for a number of I–III–*VI_2 *semiconductors crystallizing in the chalcopyrite structure at 300 K. The* E_g *versus* a_{eff} *data for CZTS and CZTSe quaternaries are also shown by the open circles. The shaded region indicates an optimal* E_g *range (~1.0–1.7 eV) in the SQ efficiency limit (see Figure 1.3). (b) Spectral irradiance (SI) for sunlight at AM1.5*

alloy bowing of E_g is taken into consideration for such chalcopyrite semiconductor alloys. The effective cubic lattice constant a_{eff} is calculated, using the lattice parameters a and c, by

$$a_{eff} = \sqrt[3]{\frac{a^2 c}{2}} \tag{1.3}$$

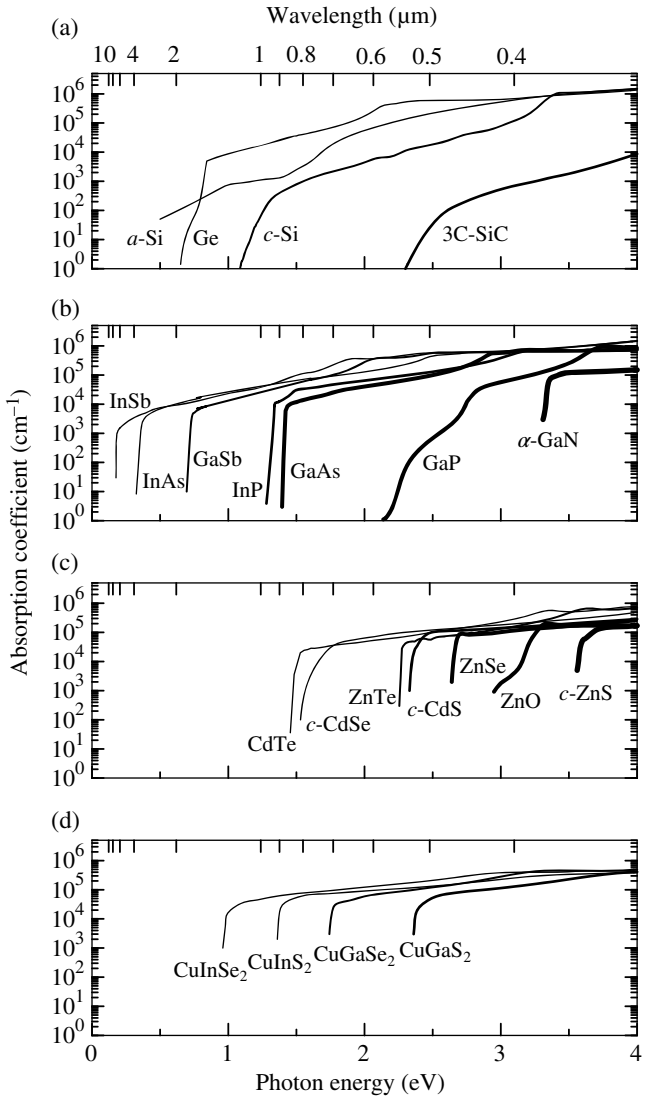

Figure 1.6 *Room-temperature optical absorption spectra* α(E) *for a number of semiconductors which are important or to be used for photovoltaic device applications: (a) group IV, (b) III–V, (c) II–VI, and (d) I–III–VI$_2$ semiconductors [5, 6]. The* α(E) *spectra for anisotropic semiconductors correspond to those for the ordinary ray* (E⊥c)

$Cu(Ga,In)Se_2$ is an alloy being used for the most efficient thin-film solar cell technology. Its endpoint material ($CuGaSe_2$ and $CuInSe_2$) values of E_g fall in an optimal band-gap range (~1.0–1.7 eV) of the SQ efficiency limit. The E_g versus a_{eff} data for CZTS and CZTSe are also plotted in Figure 1.5. An expression for a_{eff} of these quaternary materials is given in Table 2.2. Like $Cu(Ga,In)Se_2$ alloy, CZTS and CZTSe have E_g values falling in the optimal SQ efficiency limit.

The principal means of carrier generation in photovoltaic devices is the absorption of light. Figure 1.6 shows the optical absorption spectra $\alpha(E)$ of a number of semiconductors which are important or to be used for photovoltaic device applications: (a) group IV, (b) III–V, (c) II–VI, and (d) I–III–VI_2 semiconductors. The experimental data are taken from Adachi [5, 6]. The absorption edge of the direct band-gap semiconductors such as GaAs and CdTe is sharper than that of the indirect band-gap materials such as *c*-Si and 3C-SiC. The fundamental absorption edge of amorphous materials like *a*-Si can be treated as the "non-direct" absorption edge rather than the direct or indirect absorption edge [7]. However, this treatment ultimately provides a formula that is almost identical to that of the indirect absorption edge. Thus, the $\alpha(E)$ spectrum at the fundamental absorption edge of *a*-Si gradually increases with increasing E as in *c*-Si (Figure 1.6a).

Ge is an indirect band-gap semiconductor; however, it has the lowest direct band gap near 0.795 eV at 300 K that is close to the lowest indirect band gap near 0.67 eV. Thus, much stronger dipole transitions taking place at the Γ point make this indirect band-gap semiconductor as a direct band-gap semiconductor in nature. GaP is a suitable material to investigate some of the indirect band-gap semiconductor properties, since it has three indirect band gaps, near 2.26 eV ($\Gamma_8 \rightarrow X_6$), 2.48 eV ($\Gamma_8 \rightarrow X_7$), and 2.63 eV ($\Gamma_8 \rightarrow L_6$) at 300 K, which are well separated from the lowest direct band gap ($\Gamma_8 \rightarrow \Gamma_6$) at 2.76 eV. A gradual increase in the absorption coefficient can be found for the experimental data of *c*-CdSe (Figure 1.6c). This may come from an effect of the crystalline imperfections introduced during crystal growth. Note that CdSe usually crystallizes in the wurtzite structure (*w*-CdSe). Recent crystal growth technique, however, enabled to synthesize unusual polytypic crystals. The $\alpha(E)$ data of *c*-CdSe plotted in Figure 1.6c are obtained from an epitaxial sample grown on (001) GaAs by MBE. For E well above the fundamental absorption edge, all the semiconductors in Figure 1.6 show saturated absorption values in the range of $\alpha \sim 10^5 - 10^6\,cm^{-1}$.

1.5 Solar Cell Device Characteristics

Figure 1.7 shows the spectral efficiency of several different kinds of solar cells, together with the solar irradiance spectrum. Although the absolute conversion efficiencies depend on the type of solar cells, their curves are understood to reflect the solar irradiance spectrum. If we consider a multijunction solar cell, a combination of a GaInP and/or a GaAs cell with a *c*-Si solar cell appears to be an excellent combination, because the spectral efficiency of the III–V solar cells is much higher at short wavelength, while the *c*-Si solar cell exhibits best performance at long wavelengths [8]. It is also understood that an *a*-Si solar cell can hardly increase the device efficiency when combined with a *c*-Si solar cell, but should be a good combination with a μc-Si solar cell. If Si is alloyed with carbon in a layer, the band-gap energy increases and more blue light can be absorbed. Conversely, if Si is alloyed with

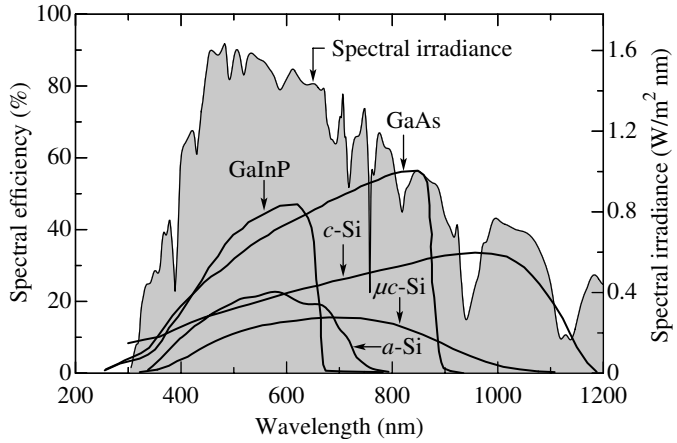

Figure 1.7 *Spectral efficiency for some different kinds of solar cells along with the spectral irradiance at AM1.5*

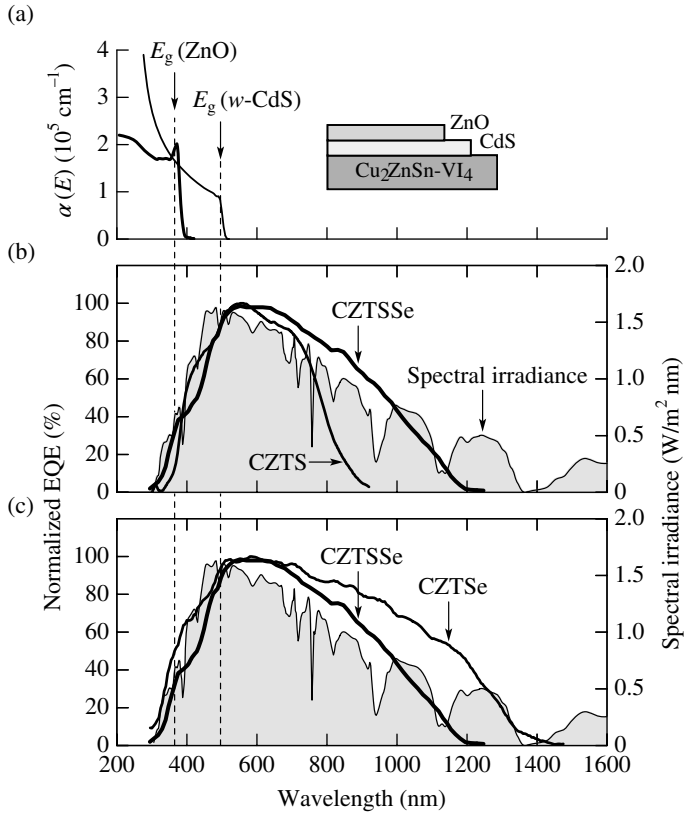

Figure 1.8 *(a) Optical absorption spectra* α(E) *for* w-*CdS and ZnO [5, 6], (b) normalized EQE of CZTS and CZTSSe solar cells, and (c) normalized EQE of CZTSe and CZTSSe solar cells. The spectral irradiance at AM1.5 is shown in (b) and (c). The experimental photovoltaic characteristics of CZTS, CZTSSe, and CZTSe solar cells are taken from Ennaoui* et al. *[9], Woo* et al. *[10], and Repins* et al. *[11], respectively*

Ge in another layer, the band-gap energy is decreased and more red lights can be absorbed. Detailed material properties of semiconductor alloys are found in Adachi [4].

Figure 1.8 shows (a) the optical absorption spectra $\alpha(E)$ of *w*-CdS and ZnO, (b) normalized EQE of CZTS and CZTSSe solar cells, and (c) normalized EQE of CZTSe and CZTSSe solar cells. The experimental absorption spectra $\alpha(E)$ of *w*-CdS and ZnO are taken from Adachi [5, 6]. The photovoltaic characteristics of CZTS, CZTSSe, and CZTSe solar cells are taken from Ennaoui *et al*. [9], Woo *et al*. [10], and Repins *et al*. [11], respectively. These solar cell devices had layers of chemical-bath-deposited *n*-type CdS and sputter-deposited ZnO on *p*-CZTS, *p*-CZTSSe, or *p*-CZTSe layer. The *n*-type CdS layer was deposited to form a *pn* heterojunction with the *p*-type CZTS, CZTSSe, or CZTSe layer. The deposition of such wide-band-gap II–VI semiconductor layers made possible expanding optical transmittance in the shorter-wavelength region, as can be understood in Figure 1.8.

1.6 Prediction of Physical Properties for Complex Material System

1.6.1 An Effective Medium Approximation

Almost all Cu_2–II–IV–VI_4 semiconductors were grown in the form of films, though a very few works grew such multinary semiconductors in the single-crystalline ingot form (see Nagaoka *et al.* [12]). A factor that can significantly influence the material properties is surface microroughness or voids present in the films. As shown in Figure 1.9, surface microroughness can be characterized by mean height of irregularities about an average and a correlation length between irregularities. Thus, the roughened surface layer on a substrate can be regarded as a physical mixture of voids and dense film material with an apparent thickness of *d*. An EM approximation or an EM theory pertains to theoretical or analytical modeling such as composite film and bulk materials.

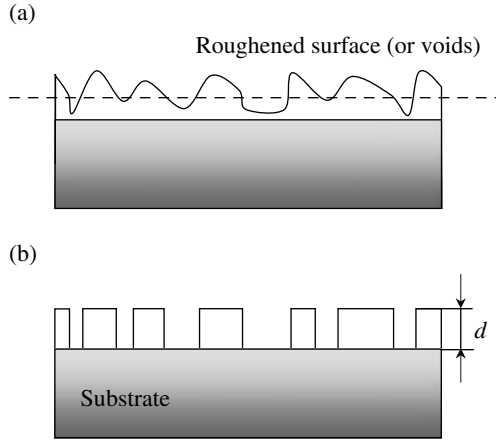

Figure 1.9 *(a) A roughened surface and (b) its equivalent EM layer thickness* d *on a substrate of the original material*

Simple approaches to the description of the material properties of a multiphase mixture were given by Lorentz and Lorenz (Lorentz–Lorenz), Maxwell and Garnet (Maxwell–Garnet), and Bruggeman [13–16]. They all have the same generic form:

$$\frac{<\varepsilon> - \varepsilon_h}{<\varepsilon> + 2\varepsilon_h} = f_1 \frac{\varepsilon_1 - \varepsilon_h}{\varepsilon_1 + 2\varepsilon_h} + f_2 \frac{\varepsilon_2 - \varepsilon_h}{\varepsilon_2 + 2\varepsilon_h} + \cdots \tag{1.4}$$

where $<\varepsilon>$, ε_h, ε_1, ε_2, … are the material parameters of the effective medium, host medium, and inclusions of types 1, 2, …, in the host, respectively. f_1, f_2, … represent the volume fractions of inclusions, 1, 2, …, in the total volume. As we will see next, the primary difference in the Lorentz–Lorenz, Maxwell–Garnet, and Bruggeman EM approximation models is the choice of the "host" medium.

We consider, as an example, the dielectric permittivity of the complex multiphase materials. The Lorentz–Lorenz EM approximation was developed to describe point polarizable entities of polarizability α embedded in vacuum. In this case, $\varepsilon_h = 1 + i0$ (vacuum) and Equation 1.4 can be written as

$$\frac{<\varepsilon> - 1}{<\varepsilon> + 2} = f_1 \frac{\varepsilon_1 - 1}{\varepsilon_1 + 2} + f_2 \frac{\varepsilon_2 - 1}{\varepsilon_2 + 2} \tag{1.5}$$

The dielectric constant ε of a medium containing a mixture of dipoles, with the ith type having polarizability α_i and occurring with a density N_i, can be given by the Clausius–Mossotti relation:

$$\frac{\varepsilon - 1}{\varepsilon + 2} = \frac{1}{3} \sum_i N_i \alpha_i \tag{1.6}$$

Thus, the Lorentz–Lorenz EM expression is expressed in terms of α_i's, which are related by the Clausius–Mossotti relation of Equation 1.6.

The Maxwell–Garnet EM approximation corresponds to macroscopic dielectric inclusions in a host dielectric background, and the quantities in Equation 1.4 have their obvious interpretations. In the case of a single inclusion in a host background, this equation becomes

$$\frac{<\varepsilon> - \varepsilon_h}{<\varepsilon> + 2\varepsilon_h} = f_1 \frac{\varepsilon_1 - \varepsilon_h}{\varepsilon_1 + 2\varepsilon_h} \tag{1.7}$$

Equation 1.7 degenerates to the Lorentz–Lorenz form if the host happens to be vacuum or air. This is then not a bad approximation if the inclusions make up a small fraction of the total volume.

For a single type of inclusion in a single host, $<\varepsilon>$ has different values in the Maxwell–Garnet EM approximation if the role of host and inclusion is interchanged—even if the respective volume fractions stay the same. To avoid this ambiguity in bulk applications, Bruggeman suggested replacing ε_h in Equation 1.4 with $<\varepsilon>$, that is, letting the EM itself acts as host medium. Under this assumption, Equation 1.4 becomes

$$\sum_{i=1}^{n} f_i \frac{\varepsilon_i - <\varepsilon>}{\varepsilon_i + 2<\varepsilon>} = 0 \tag{1.8}$$

with

$$\sum_{i=1}^{n} f_i = 1.0 \tag{1.9}$$

This is known as the Bruggeman EM approximation. This approximation gives a rigorous result of self-consistency that can be shown to be varied under fairly general conditions [15].

1.6.2 An Interpolation Scheme

A chemical compound is a substance consisting of two or more chemical elements that are chemically combined in fixed proportions. The ratio of each element is usually expressed by chemical formula. For example, water is a compound consisting of two hydrogen atoms bonded to an oxygen atom (H_2O). The atoms within a compound can be held together by a variety of interactions, ranging from covalent bonds to electrostatic forces in ionic bonds. A continuum of bond polarities exists between the purely covalent and ionic bonds. For example, H_2O is held together by polar and covalent bonds. Sodium chloride (NaCl) is an example of an ionic compound. H_2O and NaCl are binary compounds, whereas $CaCO_3$ and Cu_2SnS_3 are ternary compounds. CZTS is one of the Cu_2–II–IV–VI_4 quaternary compounds.

An alloy is a combination, either in solution or compound, of two or more elements. An alloy with two components is called a binary alloy; one with three is a ternary alloy; one with four is a quaternary alloy; one with five is a pentanary alloy. The resulting alloy substance usually has properties significantly different from those of its components. The proportions of the ingredients are available.

Simply, an alloy is formed from a physical mixture of two or more substances, whereas a compound is formed from a chemical reaction. An alloy crystal is sometimes called a mixed crystal or a solid solution. For example, GaAs is a compound consisting of Ga atoms bonded to As atoms. It is not an alloy. $Al_xGa_{1-x}As$ is a ternary alloy compound consisting of AlAs and GaAs with a mole ratio of $x : (1 - x)$. The bonds in AlAs and GaAs are not adequately described by any of these extreme types, but have characteristics intermediate to those usually associated with the covalent and ionic terms. The bonds in silicon, Si—Si, can be described by the covalent bond term only. It is an elemental semiconductor, not a compound semiconductor. Similarly, C (diamond), Ge, and Sn (gray tin) are elemental semiconductors.

Like $Al_xGa_{1-x}As$, Si_xGe_{1-x} $(0 \le x \le 1.0)$ is an alloy semiconductor. The bonds Si—Ge, Si—Si, and Ge—Ge in Si_xGe_{1-x} are, therefore, described by the covalent term only. It should be noted, however, that silicon carbide (SiC) is a compound, not a binary alloy. This is because that the chemical bonds in SiC cannot be described only by the covalent term, but have characteristics intermediate to those associated with the covalent and ionic terms, like AlAs and GaAs.

If one uses the liner interpolation scheme, the binary material parameter B for an alloy of the form A_xB_{1-x} can be derived from binary parameters (B) by [4]

$$B(x) = xA_A + (1-x)A_B \equiv a + bx \tag{1.10}$$

where $a \equiv A_A$ and $b \equiv A_A - A_B$. Some material parameters, however, deviate significantly from the liner relation of Equation 1.10, exhibiting an approximately quadratic dependence on x. The binary material parameter in such a case can be very efficiently approximated by the relationship

$$B(x) = xA_A + (1-x)A_B + x(1-x)C_{A-B} \equiv a + bx + cx^2 \tag{1.11}$$

where $a \equiv A_B$, $b \equiv A_A - A_B + C_{A-B}$, and $c \equiv -C_{A-B}$. The parameter c is called a bowing parameter.

The essentially same expressions can be obtained for a ternary alloy semiconductor in the form of $A_xB_{1-x}C$:

$$T(x) = xB_{AC} + (1-x)B_{BC} \equiv a + bx \tag{1.12}$$

$$T(x) = xB_{AC} + (1-x)B_{BC} + x(1-x)C_{A-B} \equiv a + bx + cx^2 \tag{1.13}$$

where $a \equiv B_{BC}$, $b \equiv B_{AC} - B_{BC} + C_{AB}$ ($b \equiv B_{AC} - B_{BC}$), and $c \equiv -C_{A-B}$ ($c \equiv 0$). The parameter c is a ternary bowing parameter. The material parameters of a quaternary alloy in the form of $A_xB_{1-x}C_yD_{1-y}$ or $A_xB_yC_{1-x-y}D$ $\left(AB_xC_yD_{1-x-y}\right)$ can also be given in a variety of interpolation expressions [4].

CZTS can be regarded as a quasibinary material:

$$Cu_2ZnSnS_4 \leftrightarrow Cu_2S + ZnSnS_3 \tag{1.14}$$

or

$$Cu_2ZnSnS_4 \leftrightarrow Cu_2SnS_3 + ZnS \tag{1.15}$$

Similarly, this quaternary compound can be regarded as a quasiternary material:

$$Cu_2ZnSnS_4 \leftrightarrow Cu_2S + ZnS + SnS_2 \tag{1.16}$$

or

$$Cu_2ZnSnS_4 \leftrightarrow 2CuS + ZnS + SnS \tag{1.17}$$

Using the linear interpolation scheme, the effective cubic lattice constant of CZTS can be expressed from Equation 1.14 as

$$a_{eff}(CZTS) = \frac{1}{2}a_{eff}(Cu_2S) + \frac{1}{2}a_{eff}(ZnSnS_3) \tag{1.18}$$

from Equation 1.15 as

$$a_{eff}(CZTS) = \frac{1}{2}a_{eff}(Cu_2SnS_3) + \frac{1}{2}a_{eff}(ZnS) \tag{1.19}$$

from Equation 1.16 as

$$a_{eff}(CZTS) = \frac{1}{3}a_{eff}(Cu_2S) + \frac{1}{3}a_{eff}(ZnS) + \frac{1}{3}a_{eff}(SnS_2) \tag{1.20}$$

or from Equation 1.17 as

$$a_{\text{eff}}(\text{CZTS}) = \frac{1}{2}a_{\text{eff}}(\text{CuS}) + \frac{1}{4}a_{\text{eff}}(\text{ZnS}) + \frac{1}{4}a_{\text{eff}}(\text{SnS}) \tag{1.21}$$

Table 1.4 lists the crystal system (space group), lattice constants (a, b, c), effective cubic lattice constant (a_{eff}; see Section 2.3.1), and band-gap energy (E_g) for the binary and ternary compounds quoted in Equations 1.14–1.17. There has been no report on the crystal growth of $ZnSnS_3$ ternary compound or its material properties. Only Bär *et al.* [17] reported that a Cu-poor surface layer formed by KCN etching on CZTS thin-film solar cell absorbers has a composition close to $ZnSnS_3$.

Imputing values of $a_{\text{eff}} = 0.5139$ nm (CuS), 0.5735 nm (Cu_2S), 0.54102 nm (ZnS), 0.5771 nm (SnS), 0.51432 nm (SnS_2), and 0.541 nm (Cu_2SnS_3) (see Table 1.4), one obtains the following a_{eff} values of CZTS: 0.54101 nm (Eq. 1.19), 0.5429 nm (Eq. 1.20), and 0.5365 nm (Eq. 1.21). It is understood that Equation 1.20 gives nearly the same a_{eff} value as the experimental CZTS value of $a_{\text{eff}} \sim 0.5428$ nm (Table 1.4). It should be noted,

Table 1.4 *CZTS-related binary and ternary compounds, together with their lattice constants (*a, b, c, *and* a_{eff}*) and band-gap energies (*E_g*) at 300 K*

Material	CS (SG)	Lattice constant (nm)					E_g (eV)
		a	*b*	*c*	a_{eff}	Reference	
CuS	*h* ($P6_3/mmc$)	0.3794		1.6332	0.5139	a	1.55
LT-Cu_2S	*m* ($P2_1/c$)	1.5246	1.1884	1.3494		b	1.21
HT-Cu_2S	*c* ($Fm3m$)	0.5735			0.5735	b	
LT-ZnS	*c* ($F\bar{4}3m$)	0.54102			0.54102	c	3.726
HT-ZnS	*h* ($P6_3mc$)	0.38226		0.62605	0.54112	c	3.75
SnS	*o* ($Pnma$)	0.4334	1.1200	0.3987	0.5771	d	1.049
SnS_2	*h* ($P6_3mc$)	0.36470		0.59055	0.51432	e	1.82–2.88
LT-Cu_2SnS_3	*m* (Cc)	0.665	1.154	0.667		f	0.93–1.51
	tc	0.666	1.148	2.003		f	
	t ($I\bar{4}2m$)	0.541		1.081	0.541	f	
	h ($P6_3/mmc$)	0.390		1.727	0.533	f	
HT-Cu_2SnS_3	*c* ($F\bar{4}3m$)	0.543			0.543	f	
CZTS	*t* ($I\bar{4}$)	0.5430		1.0845	0.5428	*	1.49

c, cubic; CS (SG), crystal structure (space group); *h*, hexagonal; *m*, monoclinic; *o*, orthorhombic; *t*, tetragonal; *tc*, triclinic.
[a] S. Djurle, "X-ray study of Cu–S system," *Acta Chem. Scand.* **12**, 1415–1426 (1958).
[b] O. V. Parasyuk, L. V. Piskach, Y. E. Romanyuk, I. D. Olekseyuk, V. I. Zaremba, and V. I. Pekhnyo, "Phase relations in the quasi-binary Cu_2GeS_3–ZnS and quasi-ternary Cu_2S–Zn(Cd)S–GeS_2 systems and crystal structure of Cu_2ZnGeS_4," *J. Alloys Compd.* **397**, 85–94 (2005).
[c] S. Adachi, *Properties of Group-IV, III–V and II–VI Semiconductors* (John Wiley & Sons, Ltd, Chichester, 2005).
[d] T. Chattopadhyay, J. Pannetier, and H. G. von Schnering, "Neutron diffraction study of the structural phase transition in SnS and SnSe," *J. Phys. Chem. Solids* **47**, 879–885 (1986).
[e] B. Pałosz and E. Salje, "Lattice parameters and spontaneous strain in AX_2 polytypes: CdI_2, PbI_2, SnS_2, and $SnSe_2$," *J. Appl. Cryst.* **22**, 622–623 (1989).
[f] Y.-T. Zhai, S. Chen, J.-H. Yang, H.-J. Xiang, X.-G. Gong, A. Walsh, J. Kang, and S.-H. Wei, "Structural diversity and electronic properties of Cu_2SnX_3 (X = S, Se): A first-principles investigation," *Phys. Rev. B* **84**, 075213-1–6 (2011).
* Present study.

however, that the quasibinary and quasiternary representations of Equations 1.14–1.17 do not give good basis for the estimation of E_g. For example, Equation 1.17 yields

$$E_g(\mathrm{CZTS}) = \frac{1}{2}E_g(\mathrm{CuS}) + \frac{1}{4}E_g(\mathrm{ZnS}) + \frac{1}{4}E_g(\mathrm{SnS}) \sim 2.0\,\mathrm{eV} \tag{1.22}$$

which is considerably larger than the experimental CZTS value of $E_g \sim 1.49$ eV (see Table 1.4).

An alloy system $Cu_2ZnSn(S_xSe_{1-x})_4$ (CZTSSe) can be regarded as a quasibinary system:

$$Cu_2ZnSn(S_xSe_{1-x})_4 = xCu_2ZnSnS_4 + (1-x)Cu_2ZnSnSe_4 \tag{1.23}$$

or more simply

$$\mathrm{CZTSSe} = x\mathrm{CZTS} + (1-x)\mathrm{CZTSe} \tag{1.24}$$

The pentanary material parameter M(CZTSSe) can then be calculated, using the simplest interpolation scheme, from the quaternary material parameters M(CZTS) and M (CZTSe) by

$$M(\mathrm{CZTSSe}) = xM(\mathrm{CZTS}) + (1-x)M(\mathrm{CZTSe}) \tag{1.25}$$

If we consider an effect of bowing, the above equation should be modified as

$$\begin{aligned} M(\mathrm{CZTSSe}) &= xM(\mathrm{CZTS}) + (1-x)M(\mathrm{CZTSe}) + x(1-x)C_{\mathrm{CZTS-CZTSe}} \\ &= a + bx + cx^2 \end{aligned} \tag{1.26}$$

with $a \equiv M(\mathrm{CZTSe})$, $b \equiv M(\mathrm{CZTS}) - M(\mathrm{CZTSe}) + C_{\mathrm{CZTS-CZTSe}}$, and $c \equiv -C_{\mathrm{CZTS-CZTSe}}$.

If the material parameter can be given by a specific expression owing to some physical basis, it is natural to consider that the corresponding interpolation scheme may also be obeyed to this expression. The dielectric function ε is an example of such cases that follows the Clausius–Mossotti relation (see Section 1.6.1). The interpolation scheme for CZTSSe can then be given by

$$\frac{\varepsilon(\mathrm{CZTSSe})-1}{\varepsilon(\mathrm{CZTSSe})+2} = x\frac{\varepsilon(\mathrm{CZTS})-1}{\varepsilon(\mathrm{CZTS})+2} + (1-x)\frac{\varepsilon(\mathrm{CZTSe})-1}{\varepsilon(\mathrm{CZTSe})+2} \tag{1.27}$$

The electron or hole effective mass $m_{e(h)}$ in a similar manner can be written as

$$\frac{1}{m_{e(h)}(\mathrm{CZTSSe})} = \frac{x}{m_{e(h)}(\mathrm{CZTS})} + \frac{1-x}{m_{e(h)}(\mathrm{CZTSe})} \tag{1.28}$$

Justification for the above expression is suggested by the effective mass transformation of the Schrödinger equation [18]

$$\left[-\frac{h^2\nabla^2}{2m_0} + \sum_r U(r-\tau)\right] \rightarrow -\frac{h^2\nabla^2}{2m_{e(h)}} \tag{1.29}$$

References

[1] C.-H. Ho, K.-Y. Lai, C.-A. Lin, G.-J. Lin, M.-K. Hsing, and J.-H. He, "Microdome InGaN-based multiple quantum well solar cells," *Appl. Phys. Lett.* **101**, 023902-1–4 (2012).

[2] C. R. Osterwald, "Microdome InGaN-based multiple quantum well solar cells," in *Solar Cells: Materials, Manufacture and Operation*, edited by T. Markvart and L. Castañer (Elsevier, Oxford, 2005), pp. 451–474.

[3] W. Shockley and H. J. Queisser, "Detailed balance limit of efficiency of *p-n* junction solar cells," *J. Appl. Phys.* **32**, 510–519 (1961).

[4] S. Adachi, *Properties of Semiconductor Alloys: Group-IV, III–V and II–VI Semiconductors* (John Wiley & Sons, Ltd, Chichester, 2009).

[5] S. Adachi, *Optical Constants of Crystalline and Amorphous Semiconductors: Numerical Data and Graphical Information* (Kluwer Academic, Boston, 1999).

[6] S. Adachi, *The Handbook on Optical Constants of Semiconductors: In Tables and Figures* (World Scientific, Singapore, 2012).

[7] S. Adachi, "Optical dispersion relations in amorphous semiconductors," *Phys. Rev. B* **43**, 12316–12321 (1991); "Calculation model for the optical constants of amorphous semiconductors," *J. Appl. Phys.* **70**, 2304–2308 (1991).

[8] J. C. Goldschmidt, C. Do, M. Peters, and A. Goetzberger, "Spectral splitting module geometry that utilizes light trapping," *Sol. Energy Mater. Sol. Cells* **108**, 57–64 (2013).

[9] A. Ennaoui, M. Lux-Steiner, A. Weber, D. Abou-Ras, I. Kötschau, H.-W. Schock, R. Schurr, A. Hölzing, S. Jost, R. Hock, T. Voß, J. Schulze, and A. Kirbs, "Cu_2ZnSnS_4 thin film solar cells from electroplated precursors: Novel low-cost perspective," *Thin Solid Films* **517**, 2511–2514 (2009).

[10] K. Woo, Y. Kim, W. Yang, K. Kim, I. Kim, Y. Oh, J. Y. Kim, and J. Moon, "Band-gap-graded $Cu_2ZnSn(S_{1-x}Se_x)_4$ solar cells fabricated by an ethanol-based, particulate precursor ink route," *Sci. Rep.* **3**, 3069-1–7 (2013).

[11] I. Repins, C. Beall, N. Vora, C. DeHart, D. Kuciauskas, P. Dippo, B. To, J. Mann, W.-C. Hsu, A. Goodrich, and R. Noufi, "Co-evaporated $Cu_2ZnSnSe_4$ films and devices," *Sol. Energy Mater. Sol. Cells* **101**, 154–159 (2012).

[12] A. Nagaoka, K. Yoshino, H. Taniguchi, T. Taniyama, and H. Miyake, "Growth of Cu_2ZnSnS_4 single crystal by traveling heater method," *Jpn. J. Appl. Phys.* **50**, 128001-1–2 (2011).

[13] R. M. A. Azzam and N. M. Bashara, *Ellipsometry and Polarized Light* (North–Holland, Amsterdam, 1977).

[14] C. G. Granqvist and O. Hunderi, "Optical properties of ultrafine gold particles," *Phys. Rev. B* **16**, 3513–3534 (1977).

[15] D. E. Aspnes, J. B. Theeten, and F. Hottier, Investigation of effective-medium models of microscopic surface roughness by spectroscopic ellipsometry," *Phys. Rev. B* **20**, 3292–3302 (1979).

[16] M. Wang and N. Pan, "Predictions of effective physical properties of complex multiphase materials," *Mater. Sci. Eng. R* **63**, 1–30 (2008).

[17] M. Bär, B.-A. Schubert, B. Marsen, S. Krause, S. Pookpanratana, T. Unold, L. Weinhardt, C. Heske, and H.-W. Schock, "Impact of KCN etching on the chemical and electronic surface structure of Cu_2ZnSnS_4 thin-film solar cell absorbers," *Appl. Phys. Lett.* **99**, 152111-1–3 (2011).

[18] J. W. Harrison and J. R. Hauser, "Theoretical calculations of electron mobility in ternary III–V compounds," *J. Appl. Phys.* **47**, 292–300 (1976).